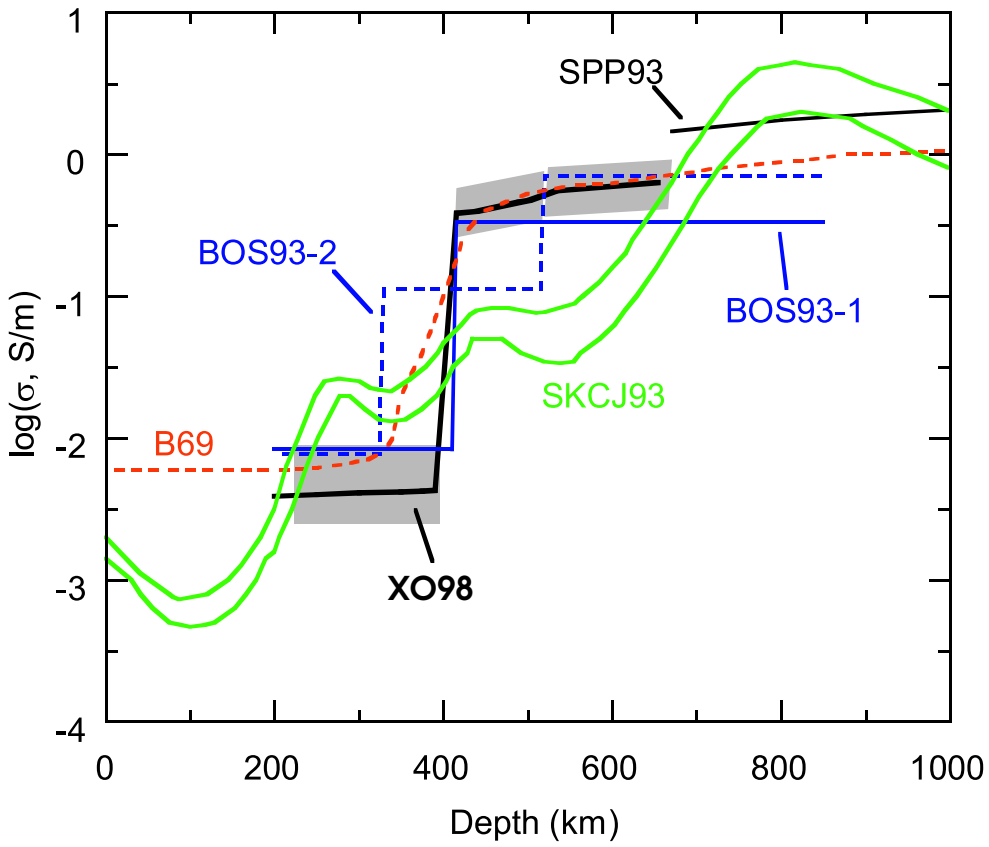

Figure 1: Layered conductivity models for the upper mantle. XO98 (thick black line) from the recent laboratory data by Xu *et al.* (1998); with the addition of a lower mantle curve SPP93 for perovskite + magnesiowüstite (Shankland *et al.*, 1993). The shaded areas illustrate the effect on the model of a ±100 k. Other geophysical models are shown as B69 (Banks, 1969), BOS93-1 and BOS93-2 (Bahr *et al.*, 1993), and SKCJ93 (Shultz *et al.*, 1993) (slightly modified from Figure 4 in Xu *et al* (1998)).

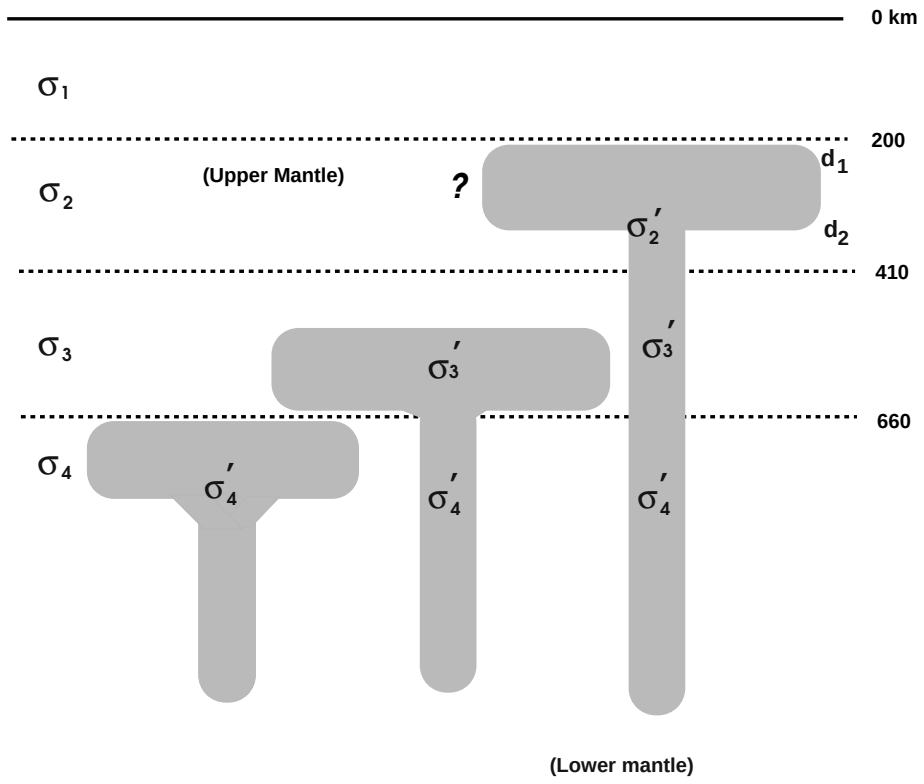

Figure 2: Illustration (will be revised) of hot plume upwelling in a narrow, vertical column (tail) with an overlying broader layer (head) in a multi-layered mantle structure. The shaded area represents a hot plume in which the conductivity (σ') is larger than outside. The depth range between d_1 and d_2 where the upwelling plume flattens is uncertain.

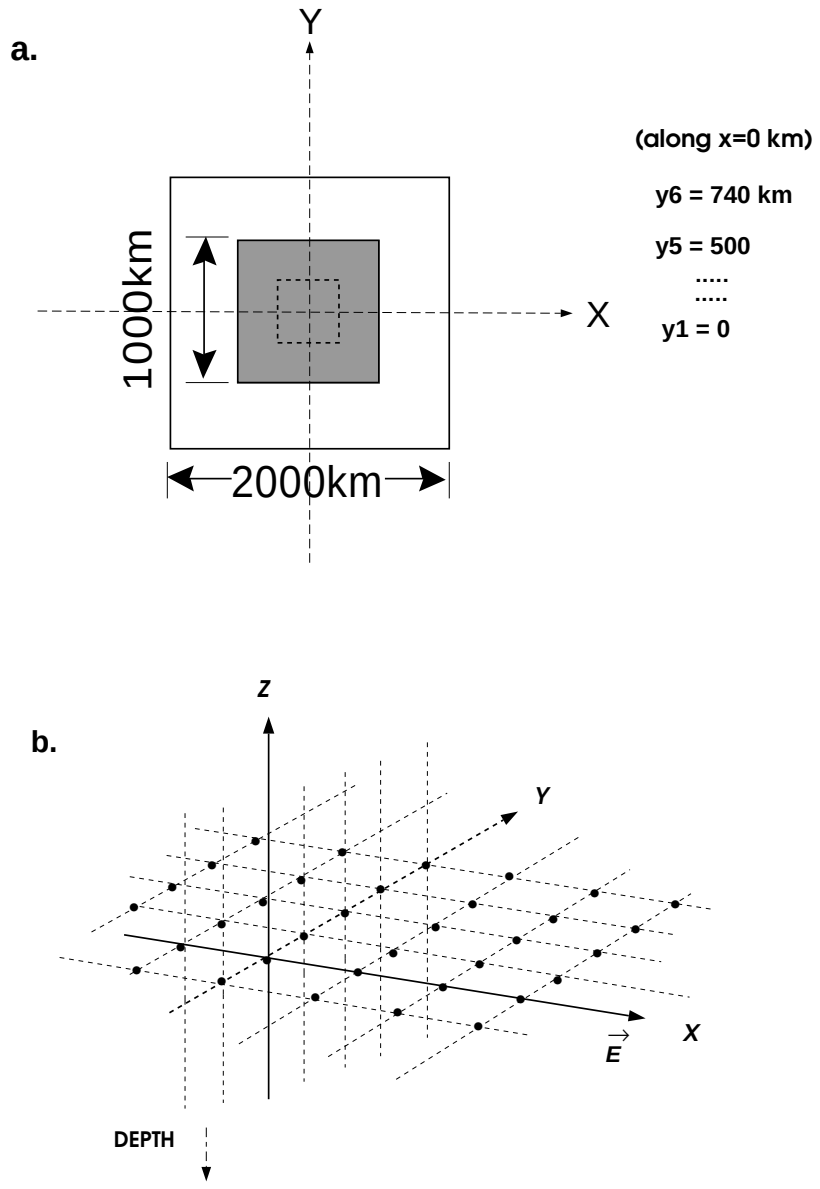

Figure 3: Grid setting for a conductivity anomaly in Cartesian coordinates. a. Conductivity anomaly (shaded area) is viewed from top. The induction evaluation positions along x=0 are y1=0, y2=100, y3=200, y4=360, y5=500, and y6=740 km, respectively (will be referred to in Figs. 5, 6, and 7). b. The grid intervals ΔX, ΔY and ΔZ are 50 km, 20 km and 10 km, respectively. The given external field $\vec{\mathbf{E}}$=(E_x,0,0) is a plane wave oscillating in the x-direction (east-west), and the induced fields $\mathbf{B_y}$ and possibly $\mathbf{B_z}$ are in the y- (north-south) and z-directions, respectively. Here the Earth's interior is in the negative z-direction.

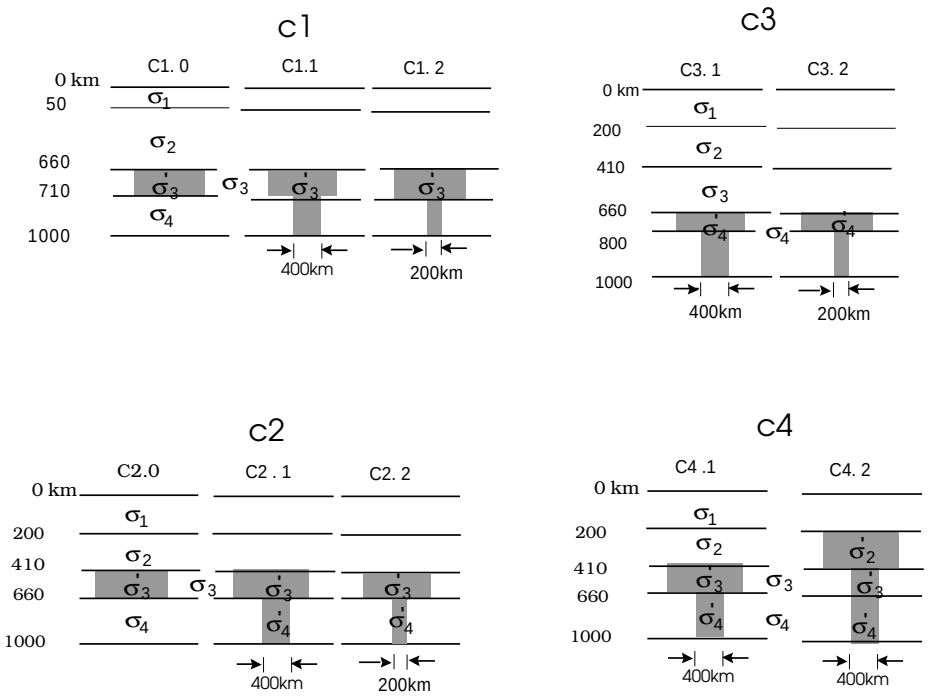

Figure 4: Schematical illustration of four layered models of electrical conductivity. C1: $\sigma_1 = 0.001$ S/m, $\sigma_2 = 0.01$ S/m, and $\sigma_3, \sigma_4 = 1$ S/m; and C2, C3, C4: the layered conductivity structure is similar to the model by Xu *et al.* (1998) (see XO98 in Fig. 1), i.e., $\sigma_1 = 0.001$ S/m, $\sigma_2 = 0.003$ S/m, $\sigma_3 = 0.3$ S/m, and $\sigma_4 = 1.6$ S/m,. The distribution of the high conductivity anomaly is varied in each model: in models C1, C2, and C3 the anomalies in the shaded areas are five times as large as the surrounding mantle, and in C4 $\sigma_2' = 15 \times \sigma_2$, $\sigma_3' = 10 \times \sigma_3$ and $\sigma_4' = 5 \times \sigma_4$.

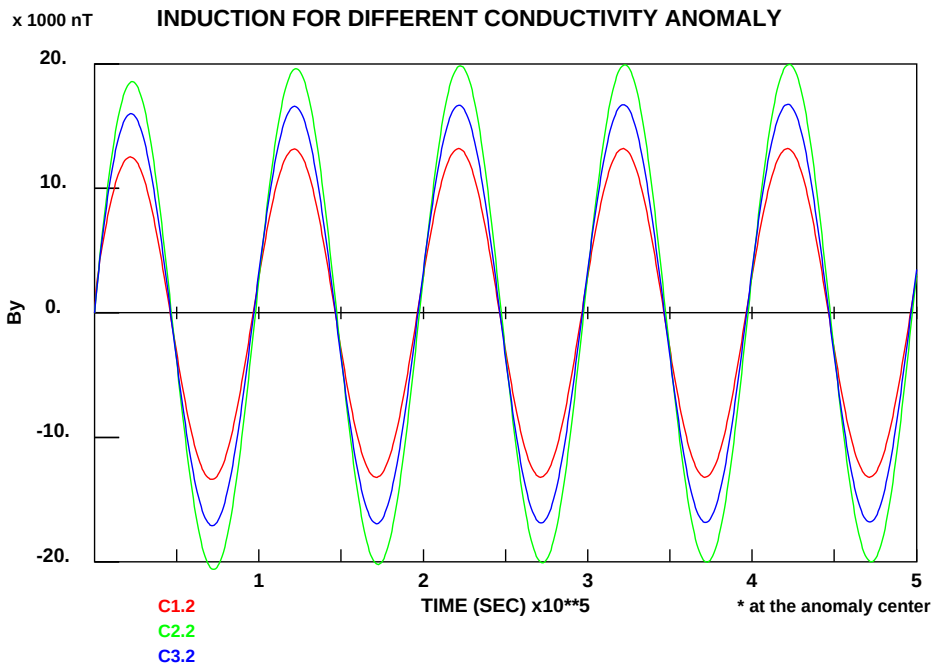

Figure 5: Induced magnetic field $\mathbf{B_y}$ in the y-direction evaluated directly above the center of conductivity anomaly ((x, y, z)= (0, 0, 0); see Fig. 3) as a function of time. The oscillation period of the input field is 100,000 sec (∼28 hours), and this diagram shows the result of computation for 500,000 sec (i.e., 5 cycles). The given conductivity anomalies are C1.2, C2.2, and C3.2 illustrated in Figure 4. The induction is stable after the third cycle and the responses are different among the models.

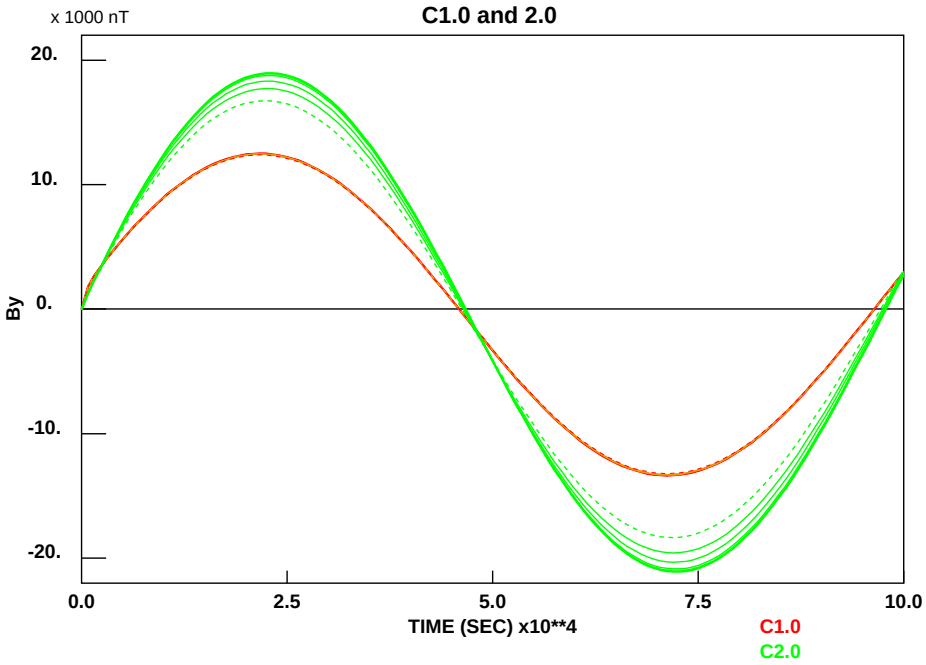

Figure 6: Induced magnetic field ($\mathbf{B_y}$) for C1.0 and C2.0 that have conductivity anomaly only in a flattened layer and no tails. The input period is also 100,000 sec and this diagram is for the first cycle. The solid lines show the responses at the center of the conductivity anomaly, i.e., at (x,y,z)=(0,0,0) (or y1=0; see Fig. 3a), the dotted lines at (x,y,z)=(0,740,0) (i.e., y6) that is outside the anomaly, and the thinner lines at locations in between. Note that the response for C2.0 is stronger than that for C1.0 and can be distinguished among the observation locations above the conductivity anomaly.

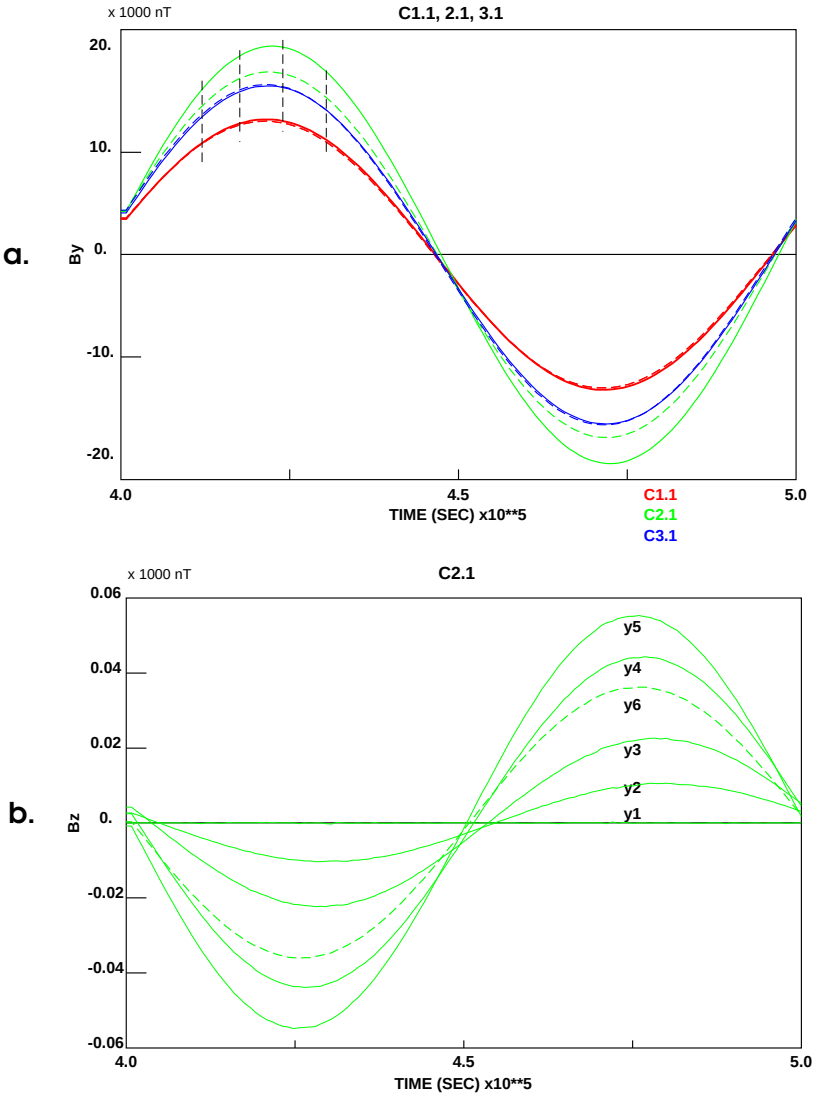

Figure 7: a. Induced magnetic fields ($\mathbf{B_y}$) in the 5-th cycle for C1.1, C2.1, and C3.1. The different model responses are obvious. The solid and dotted lines distinguish evaluation locations of induction relative to the center of the anomaly (see the text). The distinction of induction between the evaluation locations is visible for C2.1. The vertical dashed lines indicate the times when snapshots of the induced fields are taken (see Fig.8)); b. Z-component induction ($\mathbf{B_z}$) for C2.1. The maximum induction is observed just above the conductivity discontinuity (i.e., y5=500 km), and the minimum at the anomaly center. Phase shifts of induction among the locations are also observable.

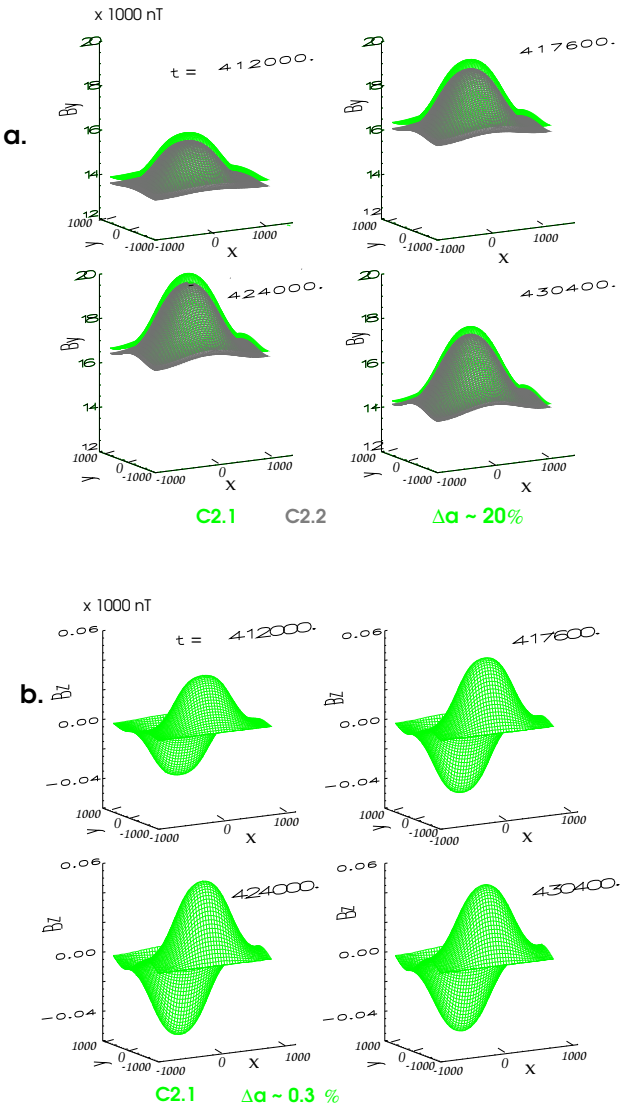

Figure 8: a. Induced magnetic field (B_y) observed at four different times (412,000s, 417,600s, 424,000s, and 430,400s) after onset. (Models C2.1 shown in green (or lighter shade) and C2.2 in shade). The diameter of the column is 400 km for C2.1 and 200 km for C2.2, respectively. The amplitude perturbation of B_y above the conductivity anomaly is $\sim$ 20% more than that outside the anomaly. b. Corresponding z-component induced magnetic field (B_z). The amplitudes are $\sim$ 0.3% of B_y. Note that without the 3-D anomaly the induced field should be a plane wave oscillating only in the y-direction, and there will be no induction in z-direction.

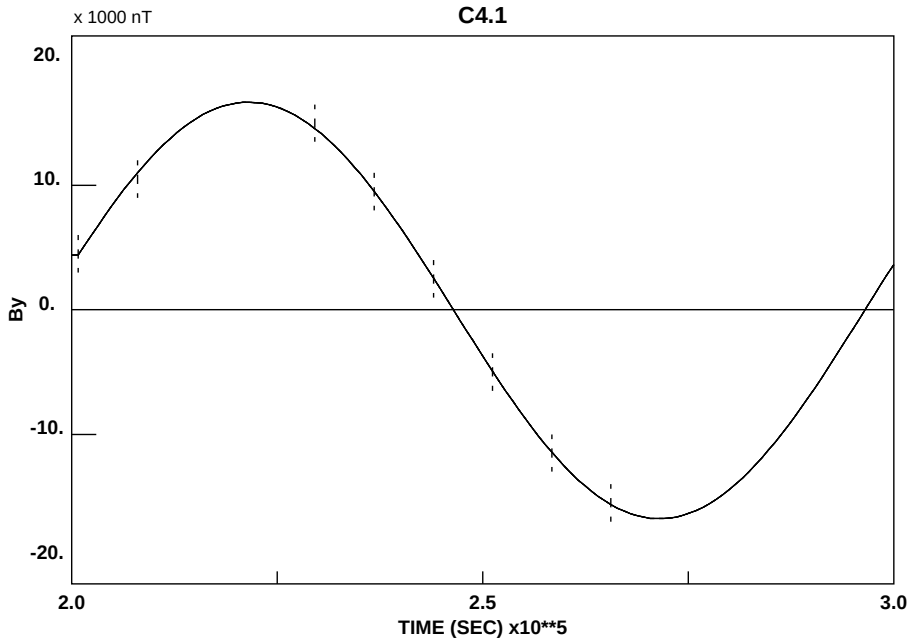

Figure 9: Induced magnetic field (B_y) for C4.1 (see Fig. 4) as a function of time in the 3rd cycle. Snapshots in Fig. 10 were made at times that are indicated with dashed lines on the disgram.

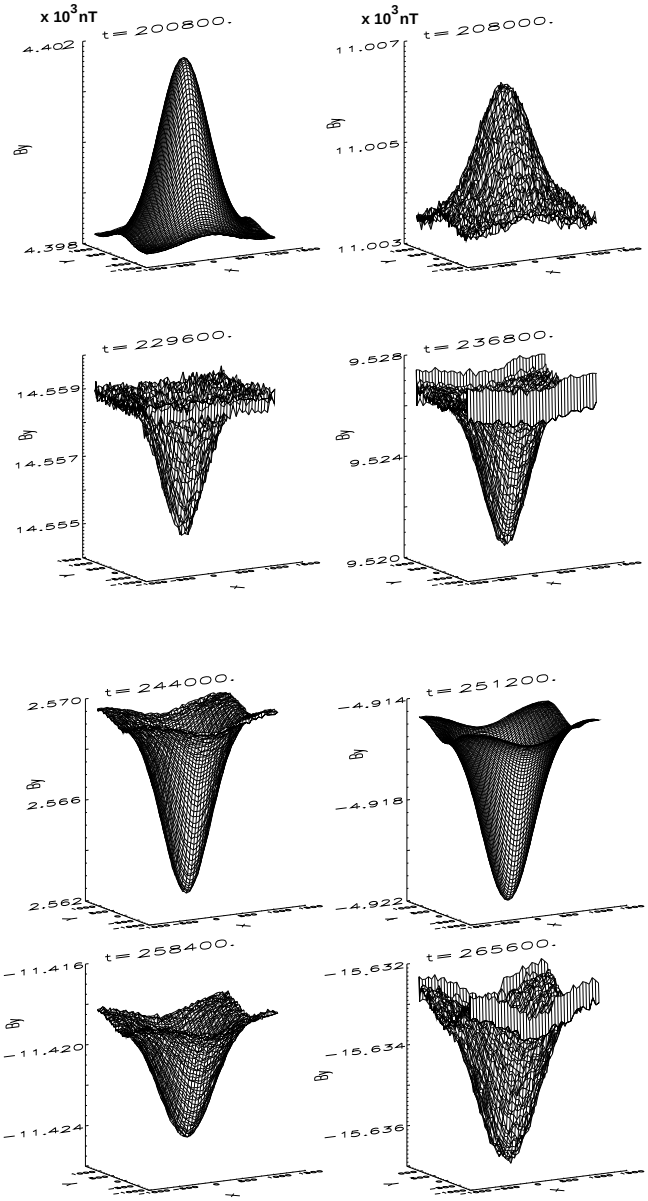

Figure 10: Perturbed induced magnetic field in the y-direction (B_y) for C4.1 (see Fig. 4). These snapshots were made at times shown with dashed lines in Fig.9 during the 3rd cycle starting at 200,800 sec after onset. The perturbation of induction B_y (either by amplification or reduction) above the anomaly is visible.